Optical and Quantum Electronics (2023) 55:1169
https://doi.org/10.1007/s11082-023-05433-0

Exploring the structural, optical, and optoelectrical characteristics of p-type $CuNiBiS_3$ thin films prepared by the chemical deposition method

H. Y. S. Al-Zahrani[1] · I. M. El Radaf[2]

Received: 2 December 2022 / Accepted: 14 September 2023 / Published online: 17 October 2023

Abstract
The authors use chemical bath deposition to synthesize novel copper-nickel bismuth sulfide ($CuNiBiS_3$) thin films on glass slides. The X-ray diffraction measurements detected the crystal structure of the $CuNiBiS_3$ layers, which display orthorhombic structures for these films. The structural indices of the $CuNiBiS_3$ layers were determined by the Williamson–Hall relationship. Furthermore, the Energy dispersive spectroscopy of the $CuNiBiS_3$ layers refers to these layers having a stoichiometric composition. On the other side, the linear optical indices of the $CuNiBiS_3$ layers were determined depending on the transmittance and reflectance data. The energy gap analysis indicates that the $CuNiBiS_3$ layers have a direct optical transition. The energy gap values of the $CuNiBiS_3$ layers were reduced from 1.43 to 1.31 eV by enlarging the thickness of these layers. These layers' nonlinear, opto-electrical, and dispersion indices, like the static high-frequency dielectric constant, optical conductivity, dispersion energy, nonlinear refractive index, and optical carrier concentration, were improved by boosting the layer thickness. Moreover, the hot probe test revealed that $CuNiBiS_3$ layers tended to acquire p-type characteristics.

Keywords $CuNnBiS_3$ thin films · Chemical deposition method · Optical properties · Nonlinear refractive index · Electrical conductivity

1 Introduction

Most scientists are now concentrating on developing efficient materials for solar energy. Despite silicon technology's commercial dominance, thin films like CdTe and Cu (In, Ga) Se_2 may present practical alternatives (Wang et al. 2021, 2022). The severe toxicity of cadmium and the scarcity of indium material present problems, though low-cost and earth-abundant materials are essential to meet the demands of researchers. The discovery has

✉ I. M. El Radaf
i.radaf@qu.edu.sa

[1] Physics Department, College of Science and Arts, King Abdulaziz University, Rabigh, Kingdom of Saudi Arabia

[2] Department of Physics, College of Science and Arts at ArRass - Qassim University, 51921 Ar Rass, Kingdom of Saudi Arabia

therefore prompted a renewed interest in metal sulfide compounds (Gao and Zhao 2022; Li et al. 2022).

Metal sulfides have received extensive study due to their applications in various devices, including lithium-ion batteries, solar cells, optical sensors, light-emitting diodes, nonvolatile memory devices, fuel cells, and thermoelectric devices. Metal sulfides are a significant group of materials that provide n-type and p-type semiconductors for research due to their various structural types since they are typically found in various forms as binary, ternary, and quaternary metal sulfides (Kajana et al. 2022; Vakalopoulou et al. 2022a; Verma et al. 2022).

Binary metal sulfide (BMS) is a great and inexpensive material that can be used in solar cells as n-type and p-type semiconductor materials. BMS such as copper sulfide (CuS), pyrite (FeS_2), zinc sulfide (ZnS), cadmium sulfide (CdS), bismuth sulfide (Bi_2S_3), and indium sulfide (In_2S_3) are abundant and inexpensive (Karsandık et al. 2022; Vakalopoulou et al. 2022b). Zinc sulfide (ZnS) is a vital metal sulfide with n-type conductivity, high transmittance, high refractive index, good chemical stability, and a wide direct bandgap. So, it can be used to create electroluminescent phosphors, sensors, photocatalysis, and light-emitting diodes (Hathot et al. 2022; Jrad et al. 2022). Copper sulfide (CuS) compound is one of the essential materials used in various applications like hydrogen storage, optoelectronic devices, photocatalysis, and photovoltaic absorbers because it has a low energy gap, p-type conductivity, and a high absorption coefficient. Further, indium sulfide (In_2S_3) drew particular attention among various chalcogenides due to its abundance on earth, nontoxicity, wider optical absorption, and narrow bandgap (Habiboglu et al. 2022; Vinotha et al. 2022).

On the other hand, ternary metal sulfide (TMS) is a significant semiconductor material that can be utilized in a variety of applications because it displays exceptional physical and chemical characteristics that make them suited for a variety of uses, such as solar panels, IR sensors, IR lasers, window coatings, energy systems, and optical fiber and light-emitting diodes (LEDs). TMS like $CuInS_2$, $CuSbSe_2$, $CuBiS_2$, $CuSbS_2$, and $CuInSe_2$ are important absorbers with narrow band gaps, p-type conductivity, and an absorption coefficient of more than 10^{-4} cm^{-1} (Chalapathi et al. 2022; Surucu et al. 2022).

Copper antimony selenide $CuSbSe_2$ is a vital absorber layer characterized by a low energy gap, abundance on earth, and p-type conductivity (Abouabassi et al. 2022; Vázquez-Barragán et al. 2022). The $CuSbSe_2$ display good photovoltaic performance in different devices. Further, high-quality p-type $CuSbSe_2$ thin films were successfully created by Elradaf et al. These films helped fabricate ITO/CdS/$CuSbSe_2$/Au solar cells that produce solar conversion efficiency of about 1.66% (El-Bana and El Radaf 2022). Also, tin-antimony sulfide ($SnSb_2S_4$) is a vital ternary chalcogenide with good optical and electrical properties. El Radaf et al. success in fabricating $SnSb_2S_4$ by spray pyrolysis procedure. This compound displays good absorption coefficients, optical conductivity, refractive index, nonlinear optical parameters, and small bandgap energy (El Radaf 2020a).

On the other side, researchers have recently concentrated on creating novel quaternary metal sulfide (QMS) thin films due to their intriguing optoelectronic, electrical, and optical characteristics. The development of QMS thin films into a new type of material has led to applications in photovoltaics, phase change materials, thin film solar cells (TFSC), optical fibers, holography, inorganic photoresists, reversible optical recording, and infrared devices (Akcay et al. 2022; Liu et al. 2022).

The Ag_2ZnSnS_4, Cu_2ZnSnS_4, and Cu_2ZnGeS_4 compositions are important QMS that exhibit interesting optical and electrical features. In prior literature, it was reported that these films exhibited good photoelectric properties as significant absorption

layers. They are also inexpensive to manufacture, stable, non-toxic, and abundant on Earth (El Radaf 2020b; El Radaf and Al-Zahrani 2020; Tian et al. 2014). According to previous studies, Ag_2ZnSnS_4 films have good optical conductivity, suitable nonlinear optical parameters, and a high absorption coefficient. So, Ag_2ZnSnS_4 films make an excellent absorber layer (Das and Mahanandia 2022).

On the other hand, Cu_2ZnSnS_4 ($CZTS_4$) is important QMS material and displays good optical and electrical performance. $CZTS_4$ thin films make an excellent absorber layer, according to prior research. The Mo/$CZTS_4$/CdS/ZnO/Al-doped ZnO/Al/LiF_2 solar cell has an efficiency of 11%, according to Chang et al. (Yan et al. 2018). On the other hand, Fouad et al. (2018) successfully created high-quality $CZTS_4$ films with good optical conductivity, nonlinear optical characteristics, and an increased absorption coefficient. The Al/n-Si/$CZTS_4$/Au heterojunction they created also had a solar efficiency of 3.37% (Fouad et al. 2018). $Cu_2ZnSnSe_4$ thin films are also adequate absorber layers for the Mo/$Cu_2ZnSnSe_4$/CdS/ZnO/Al-doped ZnO/Ni/Al/MgF_2 solar cells, which display an efficiency of 12.5% (Yin et al. 2022). Previous studies have focused on various quaternary metals sulfides like Ag_2ZnSnS_4, Cu_2ZnSnS_4, Cu_2FeSnS_4, and Cu_2MnSnS_4 thin films, but no research has been done on the physical characteristics of $CuNiBiS_3$ thin films. So, in the current study, the novel $CuNiBiS_3$ thin films are being created using the chemical bath deposition process. Also, the authors investigated the impact of layer thickness on the optoelectrical and optical characteristics and linear and nonlinear parameters.

2 Experimental details

A low-cost chemical bath deposition approach was utilized in this study to create the $CuNiBiS_3$ thin films. We initially carried out a substrate cleaning technique to produce $CuNiBiS_3$ thin films of higher quality. For cleaning, the glass sheets were submerged in pure acetone (CH_3COCH_3) in an ultrasonic bath for 15 min. Following that, the glass slides were immersed in isopropanol for 15 min. After being thoroughly cleaned with deionized water, the glass slides were air dry. Four solutions interacted with one another to form the $CuNiBiS_3$ solution: 20 ml of deionized water was dissolved in 0.06 M copper chloride ($CuCl_2$) to make the first solution. In order to make the second solution, 0.06 M nickel acetate ($Ni(OCOCH_3)_2$) was also dissolved in 20 ml of deionized water. To make the third solution, 0.06 M of bismuth nitrate ($Bi(NO_3)_3$) was dissolved in 10 ml of deionized water. In order to prepare the fourth solution, 0.18 M thiourea ($SC(NH_2)_2$ was dissolved in 60 ml of deionized water. All used chemicals are Sigma Aldrich-99.99%). The final solution's pH was raised to 11 by adding a few drops of an ammonium hydroxide solution. The glass substrates were cleaned and placed vertically inside the glass beaker at room temperature. After the chemical reaction had taken place for 3, 5, 7, and 9 h, the slides were removed from the beaker, cleaned with deionized water, and dried in the air. A Philips-X'Pert X-ray diffractometer extensively inspected the structural features of the $CuNiBiS_3$ layers. Further, the field emission scanning electron microscope (Quanta-FeG-250 USA) was utilized to study the morphology and composition of the $CuNiBiS_3$ films. On the other hand, a Shimadzu spectrophotometer (type UV-3600 Plus UV–VIS–NIR) was utilized to list the optical data in the wavelength range of 400–2500 nm.

3 Results and discussions

3.1 Morphological and XRD studies

The FESEM equipment has been used to analyse the $CuNiBiS_3$ surface morphology. Figure 1a, b, c, and d depicted the morphological characteristics of $CuNiBiS_3$ films 1 µm.

According to these FESEM micrographs, the surface of these layers is nearly homogeneous and uniform. Moreover, boosting the layer thickness enhanced the surface uniformity of the investigated layers due to the space between film grains getting less as they get bigger.

On the other hand, the chemical composition of the $CuNiBiS_3$ layers has been explored using energy-dispersive X-ray spectroscopy as presented in Fig. 2a and b. According to the reported data, the respect ratio utilized to create the $CuNiBiS_3$ samples was nearly identical to 1:1:1:3.

Figure 3 displays the XRD results of the $CuNiBiS_3$ layers deposited at different thicknesses. These illustrations show that these layers are polycrystalline, and the standard JCPDS file no. 46–1319. The displayed peaks belonged to a single $CuNiBiS_3$ phase with an orthorhombic structure.

The average crystallite sizes (D_{W-H}) and the microstrain (ε) of the $CuNiBiS_3$ layers were assessed using the Williamson–Hall (W–H) relationship (Akl et al. 2021; Akl and Hassanien 2014):

$$\beta \cos\theta = \frac{k\lambda}{D} + 4\varepsilon \sin\theta \tag{1}$$

where β refers to the experimental full width at half maximum intensity.

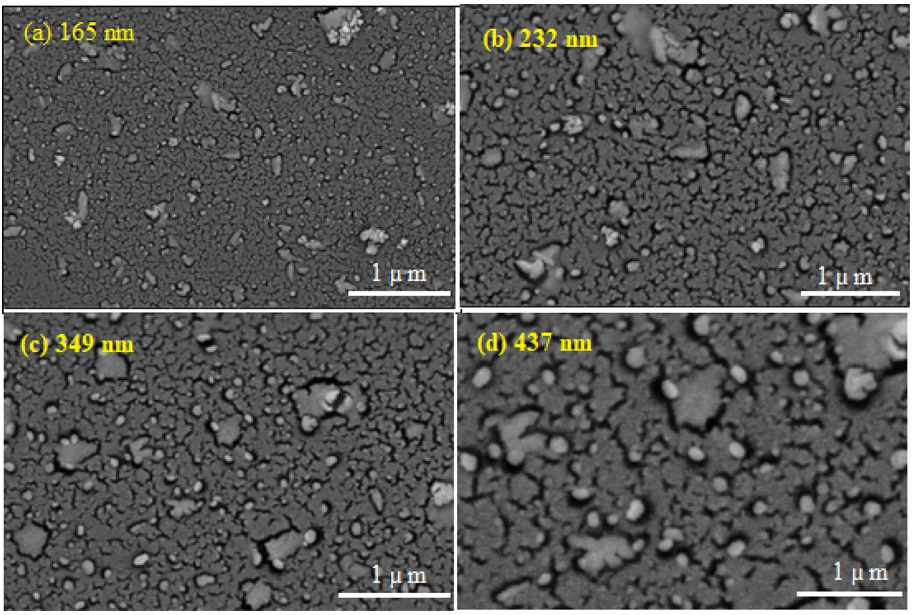

Fig. 1 SEM of the $CuNiBiS_3$ layer of thickness: **a** 165 nm, **b** 232 nm, **c** 349 and **d** 437 nm

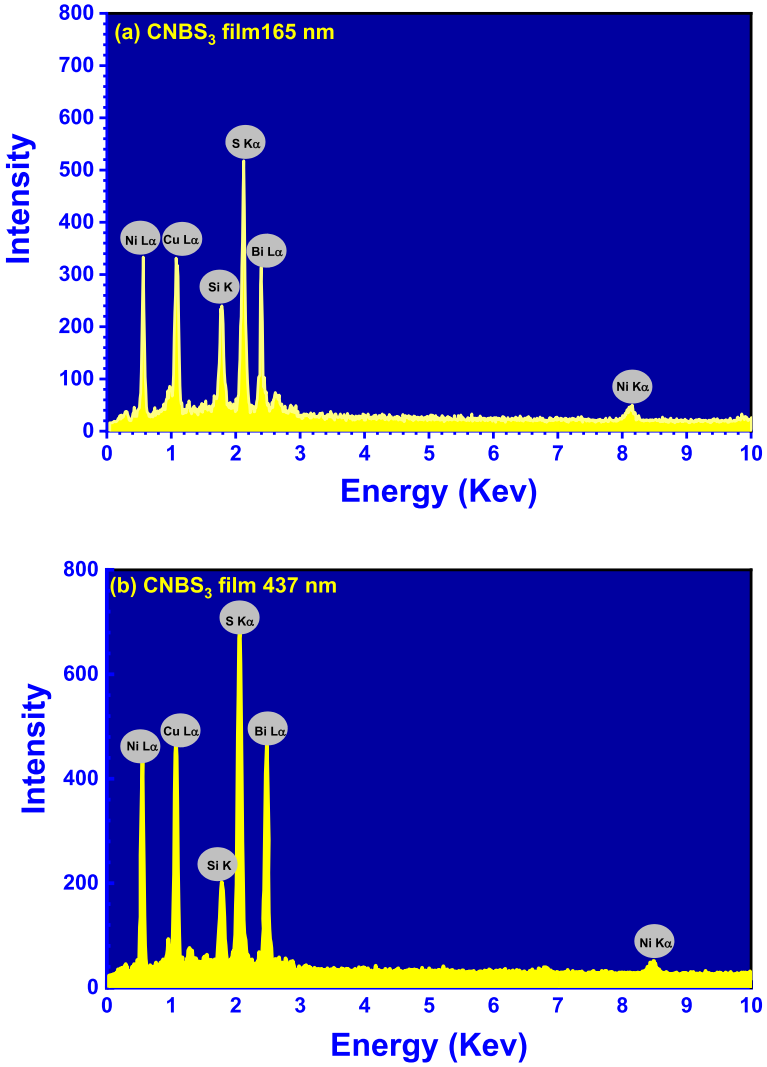

Fig. 2 EDAX spectra of the **a** $CuNiBiS_3$ layer of thickness 165 nm, **b** $CuNiBiS_3$ layer of thickness 437 nm

Using the integral breadth of the sample and the gaussian distribution function, the values of β were evaluated. Figure 4 shows the Williamson–Hall plots for the $CuNiBiS_3$ layers. According to this plot, the data points were fit to a straight line, where the slope gives the microstrain of the $CuNiBiS_3$ layers, and the inverse of the y-intercept gives the grain size of the $CuNiBiS_3$ layers. In Table 1, the D_{W-H} and ε values of the $CuNiBiS_3$ layers were recorded. This table shows how the crystallite size of the $CuNiBiS_3$ layers rose when the layer's thickness was boosted. On the other hand, as the thickness was boosted, the values of ε decreased.

Additionally, the following relationships were utilized to estimate the number of crystallites (N_C), and the dislocation density (δ) of the $CuNiBiS_3$ layers (Hassanien et al. 2021; Hathot et al. 2022):

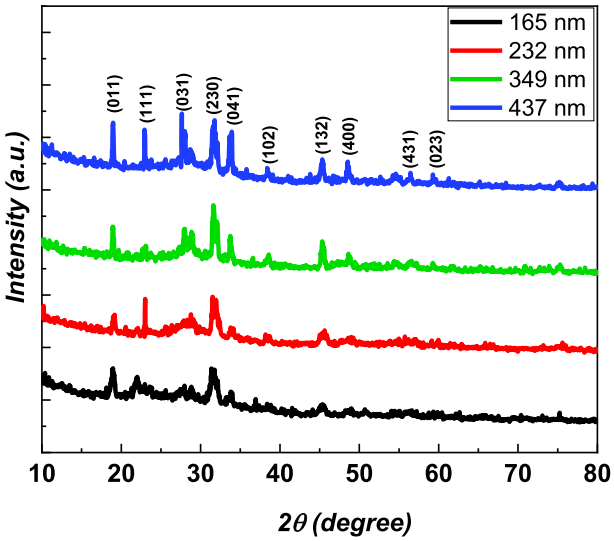

Fig. 3 XRD charts for the $CuNiBiS_3$ layers

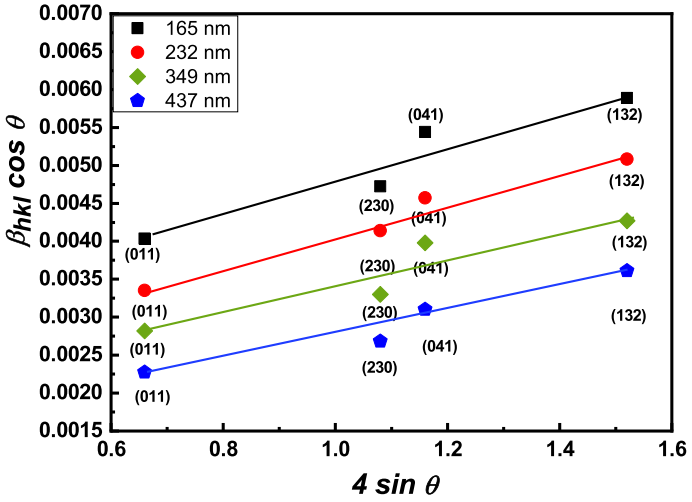

Fig. 4 The plot of 4sin(θ) against βcos (θ) for the $CuNiBiS_3$ layers

Table 1 Structural indices for the $CuNiBiS_3$ layers

t (nm)	Crystallite size, D (nm)	$\varepsilon \times 10^{-3}$	$\delta \times 10^{11}$ (Line/nm^2)	$N_C \times 10^{-2}$ (Cryst/nm^2)	
	W–H ($D_{W\text{-}H}$)	Scherrer (D_S)			
165	19.32	20.64	1.82	2.67	8.64
232	21.54	22.71	1.16	2.15	6.22
349	26.72	27.45	1.29	1.41	2.28
437	29.81	30.82	1.16	1.12	1.65

$$N_C = \frac{t}{D^3} \tag{2}$$

$$\delta = \frac{1}{D^2} \tag{3}$$

Moreover, crystallite sizes (D_S) of the $CuNiBiS_3$ layers can be evaluated using Scherer relationships (Akl et al. 2020; Akl and Hassanien 2021; Das et al. 2023; Hassanien and El Radaf 2020; Priyadarshini et al. 2021; El Radaf 2023):

$$D_S = \frac{0.9\lambda}{\beta \cos\theta} \tag{4}$$

Table 1 shows the δ, D_S, D_{W-H}, N_C, and ε for the $CuNiBiS_3$ layers, displaying that as the film thickness of the $CuNiBiS_3$ samples increased, the D_S, and D_{W-H} values were expanded while the δ, N_C, and ε values were reduced. According to this table the evaluated values of the D_S, and D_{W-H} of the $CuNiBiS_3$ layers are near to each other.

3.2 Linear optical studies

In the current work, the optical transmittance (T) and reflectance (R) of the $CuNiBiS_3$ films were obtained using a double-beam spectrophotometer. Using the T and R, the linear optical parameters of the $CuNiBiS_3$ have been computed. The T and R spectra of the novel $CuNiBiS_3$ layers in the 400–2500 nm wavelength range are shown in Fig. 5a and b. This graph shows that the $CuNiBiS_3$ layers have high optical transmittance of up to 86% and that the T of the $CuNiBiS_3$ layers is reduced by boosting the layer thickness. This trend was related to increasing the thickness of the samples increasing the absorbance value in the films, which decreased the transmittance value in the films (Behera et al. 2020; Naik et al. 2013; Naik and Ganesan 2014). Further, the R of the $CuNiBiS_3$ films improved by enlarging the layer thickness.

The absorption coefficient of the studied films is a very relevant factor that illustrates how deep into the substance can travel the light when absorbed. In this report, the

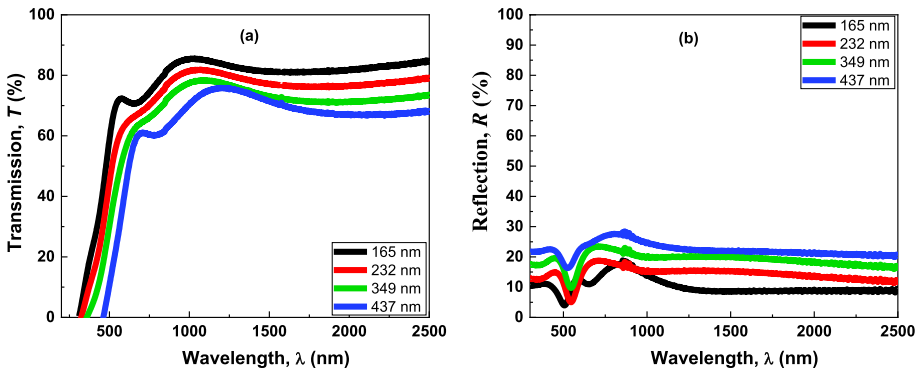

Fig. 5 **a** The spectral alterations of T as functions of λ for the $CuNiBiS_3$ samples, **b** the spectral variations of R as functions of λ for the $CuNiBiS_3$ films

absorption coefficient of the $CuNiBiS_3$ films was computed using the below formula (El Radaf and Al-Zahrani 2022):

$$\alpha = \frac{1}{d} ln \left[\frac{(1-R)^2}{2T} + \left(\frac{(1-R)^4}{4T^2} + R^2 \right)^{1/2} \right] \quad (5)$$

where d refers to the thickness of the sprayed $CuNiBiS_3$ films.

Figure 6a shows the reliance of α on the in λ for the novel $CuNiBiS_3$ films. It is revealed that the $CuNiBiS_3$ layers have large values of the α. By raising the layer thickness of the $CuNiBiS_3$ layers, the values of α were boosted.

On the other side, the energy gap (E_g) of the sprayed $CuNiBiS_3$ films was obtained by Tauc's relationship (Mohamed et al. 2019b; Qasem et al. 2020; Tauc et al. 1966):

$$\alpha h\nu = R\left(h\nu - E_g\right)^g \quad (6)$$

Here, R is Tauc parameter, and f designates the optical transition kind, either direct allowed ($g=0.5$) or indirect allowed ($g=2$).

A good match has been identified for $g=2$, indicating the allowed direct transition state. Figure 6b depicts the relationship between $(h\nu)^2$ against $h\nu$ for the novel $CuNiBiS_3$ layers. The E_g values of the novel $CuNiBiS_3$ layers are listed in Table 2. The k selection rule and the disorder-induced spatial correlation of optical transitions between the valence

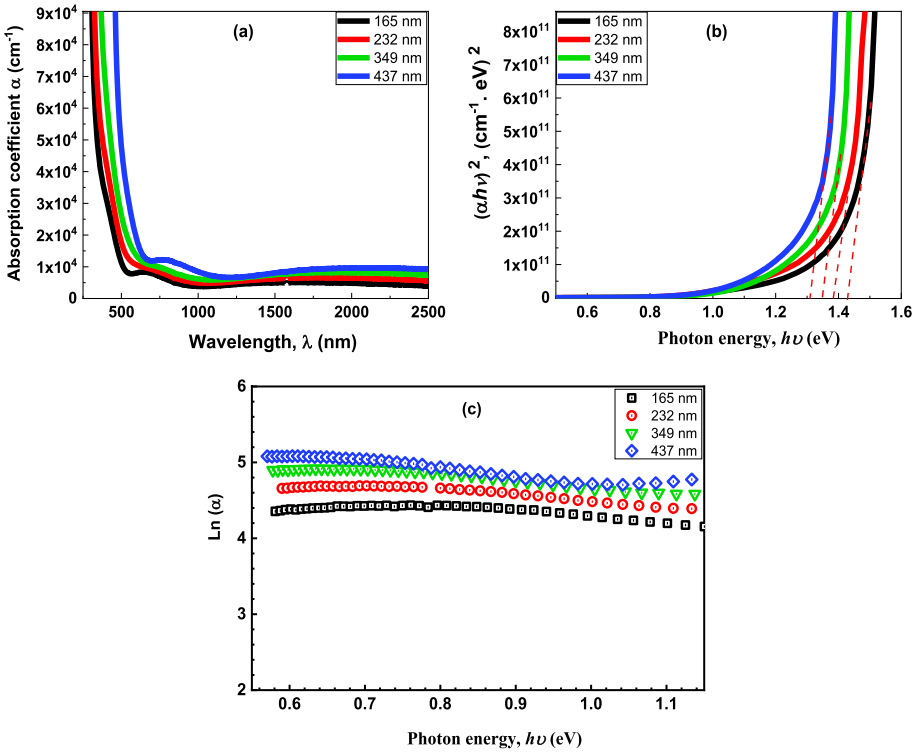

Fig. 6 **a** The absorption coefficient α of the novel $CuNiBiS_3$ layers versus λ, **b** the $(\alpha h\nu)^2$ against $h\nu$ for the $CuNiBiS_3$ samples, **c** the alteration of $ln\ (\alpha)$ with the $h\nu$ for the $CuNiBiS_3$ samples

Table 2 The optical and dispersion constants of the $CuNiBiS_3$ samples

Thickness (nm)	E_u(eV)	E_g^{dir}(eV) ± 0.17	E_o (eV)	E_d (eV)	ε_s	n_o	f
165 nm	0.16	1.43	2.75	8.12	3.95	1.98	22.33
232 nm	0.18	1.38	2.64	8.94	4.38	2.09	23.6
349 nm	0.19	1.35	2.59	9.56	4.69	2.16	24.76
437 nm	0.21	1.31	2.46	10.27	5.17	2.27	25.26

and conduction bands are both reflected in the constant R, which also contains information about the convolution of the valence and conduction band states and the matrix element of optical transitions. Not only that, but R is extremely bond type dependant. When compared to the intense absorption in the band gap region, the loss due to reflection was relatively little (Ghosh et al. 2023). It is obvious that the E_g values decreased from 1.43 to 1.31 eV as the layer thickness was raised. This tendency results in the film energy gap narrowing, which may be explained by the correlation between the increasing layer thickness and the rise in localized states inside the gap (Dughaish and Mohamed 2013; Hassanien et al. 2016; Mohamed et al. 2010). Typically, film thickness increases concurrently with the creation of defects in the layer that result in localized states along the valence band and conduction band boundaries.

Additionally, we compute the Urbach energy (E_u) of the novel $CuNiBiS_3$ films using the Urbach relation (Qasem et al. 2022):

$$\alpha = \alpha_o \exp\left(h\upsilon/E_u\right) \tag{7}$$

A plot of the $ln\ (\alpha)$ of the innovative $CuNiBiS_3$ films against hν is provided in Fig. 6c. This graph indicates how the values of E_u for $CuNiBiS_3$ films can be obtained using the slope of a straight line. Likewise, Table 2 lists the E_u of the novel $CuNiBiS_3$ films. It is apparent from the table that the E_u values increased as the film thickness. This trend was related to increasing the annealing the number of defect states in the confined region and the degree of disorder, both of which lead to a smaller band gap, as reported by this and other studies (Naik et al. 2009; Sahoo et al. 2020).

Furthermore, the extinction coefficient of the novel $CuNiBiS_3$ layers (k) was computed by the below formula (Hassanien et al. 2020b):

$$k = \frac{\alpha\lambda}{4\pi} \tag{8}$$

Figure 7a implies the alteration of k of the $CuNiBiS_3$ layers with λ. It was evident that when thickness rose, the values of the extinction coefficient, k, were also boosted. This trend may be attributed to enlarging these samples' absorption coefficient by boosting the thickness (Mohamed et al. 2019a).

On the other side, the refractive index (n) of the novel $CuNiBiS_3$ layers was estimated according to the Kramer-Kroning relationship (El Radaf et al. 2020):

$$n = \frac{1+R}{1-R} + \left(\frac{4R}{(1-R)^2} - k^2\right)^{1/2} \tag{9}$$

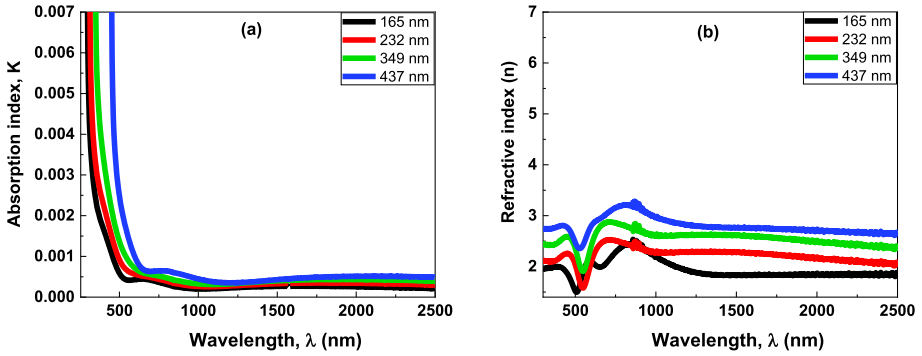

Fig. 7 **a** The relationship between the k and λ of the $CuNiBiS_3$ layers, **b** The variance of the n with λ of the $CuNiBiS_3$ layers

The variation in the n of the $CuNiBiS_3$ layers with λ is established in Fig. 7b. It is noted that the n was boosted as the layer thickness enlarged. This behavior might be ascribed to enlarging of these samples' reflectance by boosting the thickness (Naik et al. 2020).

Likewise, the Wemple–DiDomenico relations was employed to determine the dispersion parameters of the novel $CuNiBiS_3$ films (Wemple 1973; Wemple and DiDomenico 1971):

$$n^2 = 1 + \frac{E_o E_d}{E_o^2 - (h\upsilon)^2} \tag{10}$$

where E_d refers to the dispersion energy of the $CuNiBiS_3$ layers, and E_o stands for the oscillator energy of the $CuNiBiS_3$ layers.

Figure 8 illustrates the plot of the $((n^2-1)^{-1}$ versus $(h\upsilon)^2$ for the novel $CuNiBiS_3$ films. The values of the E_o and the E_d of the novel $CuNiBiS_3$ films were computed from

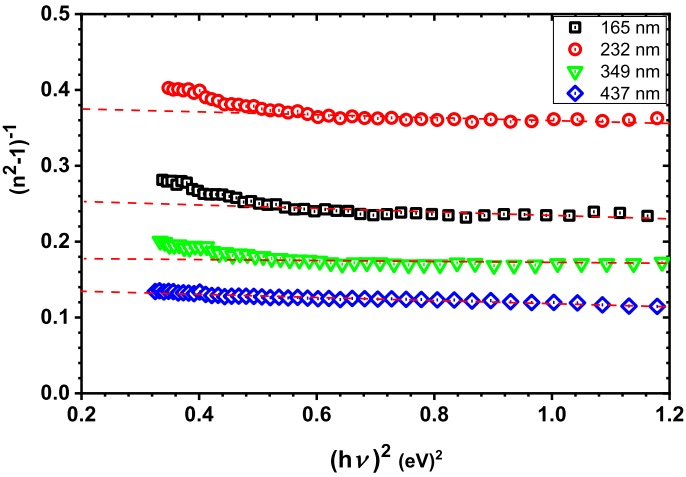

Fig. 8 The alteration of $\left(n^2-1\right)^{-1}$ as function of $(h\nu)^2$ for the $CuNiBiS_3$ layers

this plot. Table 2 lists the values of the E_o and the E_d of the novel $CuNiBiS_3$ films. According to this table, E_d values climbed while E_o values dropped as film thickness grew.

Additionally, we compute the oscillator parameter of the novel $CuNiBiS_3$ films (the static high-frequency dielectric constant, ε_s refers to the static refractive index, n_o and the oscillator strength, f) by the Wemple-DiDomenico relations (Aly 2010; Hassanien 2016; Mohamed et al. 2019a):

$$f = E_o E_d \tag{11}$$

$$n_o = \sqrt{1 + \frac{E_d}{E_o}} \tag{12}$$

$$\varepsilon_s = n_o^2 \tag{13}$$

Table 2 shows the magnitudes of the ε_s, n_o and f of the novel $CuNiBiS_3$ layers. It can be detected that as the layer thickness of the $CuNiBiS_3$ layers boosted, the ε_s, $n_{o,}$ and f values were enlarged.

3.3 Optoelectrical characterization

The optoelectrical characteristics of the substances under study, such as lattice dielectric constant, optical carrier concentration, optical conductivity, plasma frequency, and electrical conductivity, play a critical role in assessing whether the materials will be employed in optoelectronic devices. In this paper, the below optoelectrical relations were employed in order to evaluate the lattice dielectric constant ε_L, plasma frequency ω_p, and the values of charge carrier concentration to effective mass ratio N_{opt}/m^* of the $CuNiBiS_3$ films (Sharma et al. 2022; Sharma and Katyal 2008):

$$n^2 = \varepsilon_L - \left(\frac{e^2}{4\pi^2 c^2 \varepsilon_0}\right)\left(\frac{N_{opt}}{m^*}\right)\lambda^2 \tag{14}$$

$$\omega_p = \sqrt{\frac{e^2 N_{opt}}{\varepsilon_0 \varepsilon_\infty m^*}} \tag{15}$$

where ε_0 refers to the free space electric permittivity, c stands for the speed of light, e stands for the electronic charge.

The fluctuations of n^2 versus λ^2 for the $CuNiBiS_3$ films can be seen in Fig. 9a. From this plot, we deduce the $\left(N_{opt}/m^*\right)$ and ε_L values. Table 3 provides the values of the $\left(N_{opt}/m^*\right)$ and ε_L. It has been established that as the film thickness is raised, the $\left(N_{opt}/m^*\right)$ enlarged. This performance could possibly be attributed to the rise in lone-pair electrons of sulfur atoms in the layer. On the other hand, as the film thickness is raised, the values of ε_L improve. The possibility of ordering $CuNiBiS_3$ films, which would improve the film's atom arrangement in comparison to other investigated films, may be the cause of this pattern. The in ε_L value of the studied layers enlarged. Moreover, the values of ω_p of the $CuNiBiS_3$ layers reduced by enlarging the layer thickness.

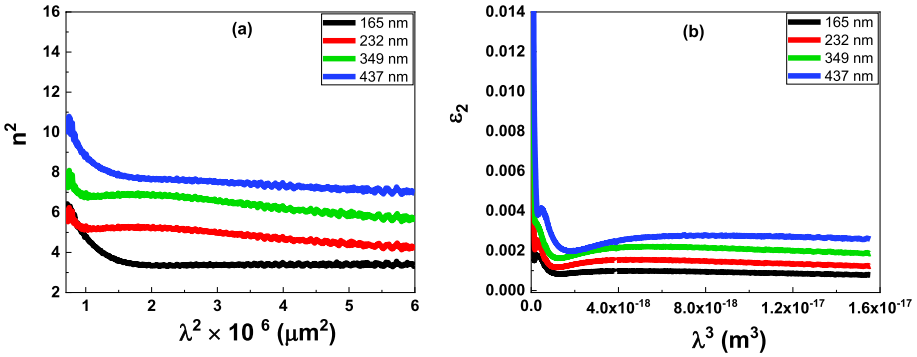

Fig. 9 **a** The variation of n^2 with λ^2 for the $CuNiBiS_3$ layers, **b** the credence of the ε_2 on λ^3 for the $CuNiBiS_3$ layers

Table 3 The optoelectrical parameters of the $CuNiBiS_3$ layers

Thickness (nm)	$N_{opt}/m^*(\times 10^{54})$ $Kg^{-1}m^{-3}$	ε_L	$\tau(\times 10^{-16})$ sec	$\omega_p(\times 10^{13})$ Hz	$\rho_{opt}(\frac{Kg.m^3}{C^2.sec})$	μ_{opt} $(\times 10^{-4})$C.sec/kg
165 nm	0.86	3.86	11.57	3.48	0.054	0.78
232 nm	1.13	4.02	8.12	3.42	0.071	2.63
349 nm	1.45	4.21	6.59	3.12	0.18	4.41
437 nm	1.58	4.49	1.98	2.85	0.23	5.94

Likewise, the relaxation time τ of the novel $CuNiBiS_3$ layers was estimated according to the below relationship (Sharma and Hassanien 2020):

$$\varepsilon_2 = \frac{1}{4\pi^3\varepsilon_0}\left(\frac{e^2}{c^3}\right)\left(\frac{N_{opt}}{m^*}\right)\left(\frac{1}{\tau}\right)\lambda^3 \tag{16}$$

Figure 9b implies the alteration of the ε_2 on the λ^3 for the $CuNiBiS_3$ films. It was evident that when thickness rose, the values of τ were reduced.

Furthermore, the following equations were employed to compute the optical resistivity and optical mobility of the $CuNiBiS_3$ films (El-Denglawey et al. 2022; Hassanien and Sharma 2021):

$$\rho_{opt} = \frac{1}{e}\mu_{opt} \tag{17}$$

$$\mu_{opt} = \frac{e\tau}{m^*} \tag{18}$$

Table 3 lists the magnitudes of the μ_{opt} and ρ_{opt} for the $CuNiBiS_3$ layers. It can be detected that as the film thickness of the $CuNiBiS_3$ layers enlarged, the μ_{opt} and ρ_{opt} values were boosted. These findings exhibit good consistency with the other papers that have already been published (Hassanien et al. 2020a).

Depending on the values of the n and α of the novel $CuNiBiS_3$ layers, the values of the optical conductivity (σ_{opt}) and the electrical conductivity (σ_e) can be estimated according to the below relations (El Radaf et al. 2018; El Radaf and Abdelhameed 2018):

$$\sigma_{opt} = \frac{\alpha nc}{4\pi} \tag{19}$$

$$\sigma_e = \frac{2\lambda\sigma_{opt}}{\alpha} \tag{20}$$

A plot of the σ_{opt} versus $h\upsilon$ for the $CuNiBiS_3$ layers can be seen in Fig. 10a. It was evident that as layer thickness expanded, optical conductivity values also steadily enlarged. The improvement of charge carriers was related to this performance. Likewise, when the incident photon energy grew, so did the optical conductivity. Increased photon energy-induced electronic charge excitation is the cause of this pattern (Wassel and El Radaf 2020).

The relationship between electrical conductivity and photon energy is seen in Fig. 10b. The graph clearly indicates that the electrical conductivity values of the $CuNiBiS_3$ films enhance with film thickness while diminishing with incident photon energy.

Additionally, we compute the imaginary and real components of the optical dielectric constant (ε_1 and ε_2) of the novel $CuNiBiS_3$ layers using the below relations (Ali et al. 2018; El Radaf et al. 2019):

$$\varepsilon_1 = n^2 - k^2 \tag{21}$$

$$\varepsilon_2 = 2nk \tag{22}$$

Figure 11a and b indicate the alteration of the ε_1 and ε_2 of the novel $CuNiBiS_3$ layers with λ. It can be observed that the ε_1 and ε_2 of the novel $CuNiBiS_3$ layers were supposedly enhanced by boosting the layer thickness. This performance may be related to enlarging the values of n and k by boosting the film thickness.

3.4 Nonlinear optical indices

On the other side, Miller's relations can also be used to predict the third-order nonlinear susceptibility $\chi^{(3)}$, the first-order nonlinear susceptibility $\chi^{(1)}$, and the nonlinear refractive

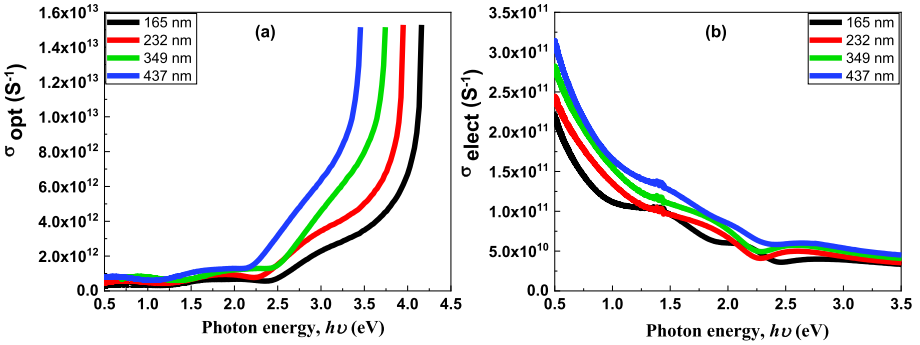

Fig. 10 **a** The alteration of the σ_{opt} with the $h\upsilon$ for the $CuNiBiS_3$ samples, **b** the σ_e against the $h\upsilon$ for the $CuNiBiS_3$ samples

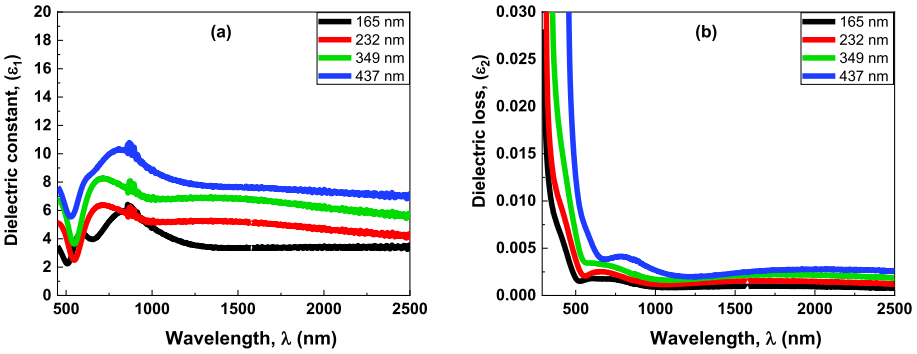

Fig. 11 **a** The plot of ε_1 against the λ for the $CuNiBiS_3$ samples, **b** the ε_2 versus the λ for the $CuNiBiS_3$ samples

index n_2 of the $CuNiBiS_3$ layers by (Alzaid et al. 2020; Hassanien 2022; Hassanien et al. 2021; Shaaban et al. 2019):

$$\chi^{(1)} = \frac{n^2 - 1}{4\pi} \tag{23}$$

$$\chi^{(3)} = B\left[\frac{n^2 - 1}{4\pi}\right]^4 \tag{24}$$

$$n_2 = \frac{12\pi\chi^{(3)}}{n_0} \tag{25}$$

Figure 12a–c indicates how the nonlinear indices of the novel $CuNiBiS_3$ films rely on the photon energy. These figures indicate that increasing the thickness of the explored layers boosted the values of the $\chi^{(1)}$, $\chi^{(3)}$, and n_2. This may be connected to the improvement in film refractive indices, which helps to expand the three-dimensional network of the films. The obtained values for the indices $\chi^{(1)}$, $\chi^{(3)}$, and n_2 are also roughly higher than those for earlier described semiconductors (Das et al. 2022; Naik et al. 2020; El Radaf 2020c; El Radaf and Al-Zahrani 2021; El Radaf and Wassel 2021; Sahoo et al. 2021a, 2021b). This would suggest that there are additional carriers in the $CuNiBiS_3$ material under study. The bound electrons' nonlinear reaction to the light's electric field in the material is enhanced.

3.5 Identifying the majority carriers in the $CuNiBiS_3$ layers

The hot-probe procedure is crucial for identifying the semiconductor type. The hot-probe technique reveals p-type conductivity in the $CuNiBiS_3$ layers. During this process, a soldering iron and a sensitive multimeter are used. Figure 13 indicates how to do a hot probe. The heated side of the $CuNiBiS_3$ film was attached to the positive multimeter terminal, which was attached to the multimeter's negative terminal. The n-type semiconductor is represented by the positive voltage that was recorded on the multimeter after the experiment, whereas the p-type semiconductor is represented by the negative voltage (Göde 2011; Golan et al. 2006). Our studies have shown that all $CuNiBiS_3$ films generate a

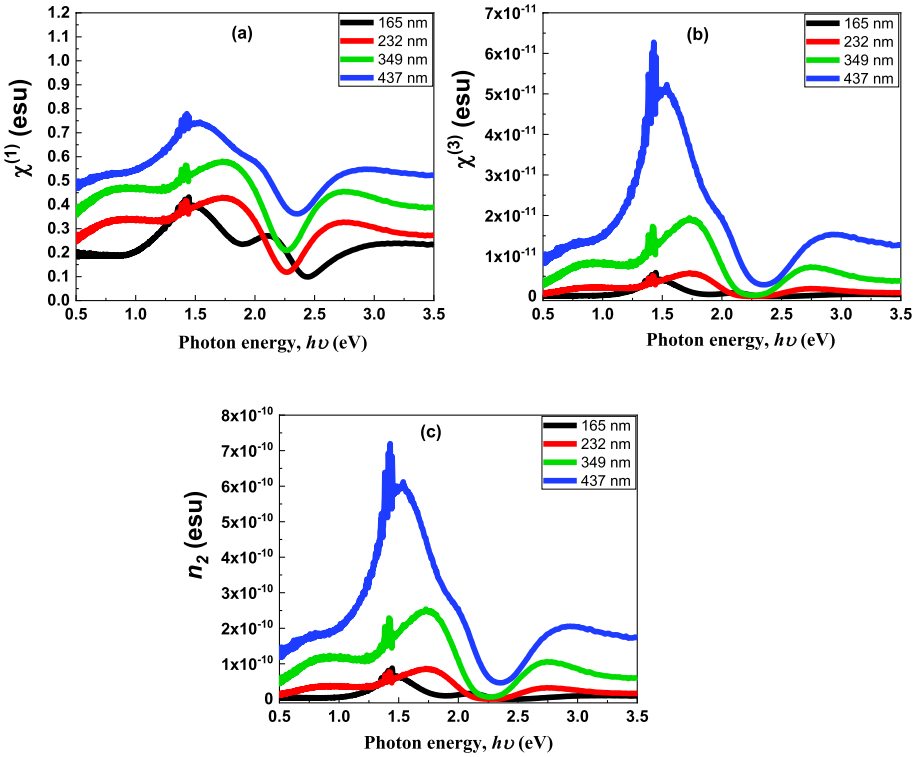

Fig. 12 **a–c**: The alteration of the $\chi^{(1)}$, $\chi^{(3)}$, and n_2 with $h\nu$ for the $CuNiBiS_3$ samples

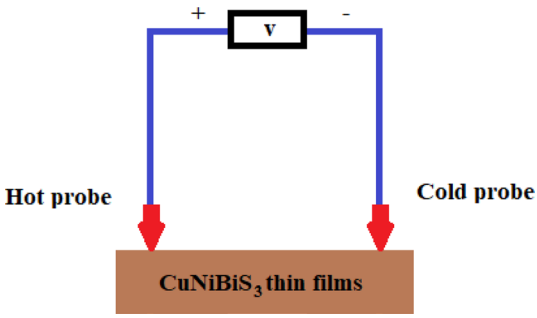

Fig. 13 The hot-probe experiment applied to the $CuNiBiS_3$ samples

negative voltage when heated. This demonstrates that the films frequently behave as p-type semiconductors.

4 Conclusion

This study presented the fabrication of the $CuNiBiS_3$ layers of various thicknesses using the chemical bath deposition method. The XRD measurements investigated the structure of the as-deposited $CuNiBiS_3$ samples to be orthorhombic. The composition of the $CuNiBiS_3$ layers was confirmed by the EDAX measurements, which show stoichiometric composition. Additionally, the novel $CuNiBiS_3$ layers show a direct energy gap, and by increasing the layer thickness from 165 to 437 nm, the energy gaps of these layers were reduced from 1.43 to 1.31 eV. The extinction coefficient, refractive index, Urbach energy, and absorption coefficient values also increased as the layer thickness was boosted. Also, increasing the thickness of the investigated layers boosted the optoelectrical indices, such as optical mobility, optical carrier concentration, optical conductivity, relaxation duration, and optical resistivity. The nonlinear optical investigation showed that enlarging the thickness improved the nonlinear optical characteristics. The hot prob method also proved the p-type semiconducting characteristics of our samples.

Acknowledgements Not applicable

Authors' contributions A-Z: Resources, writing—original draft, conceptualization, investigation, writing—review and editing, formal analysis, data curation, methodology, E: resources, writing—original draft, conceptualization, investigation, writing—review and editing, formal analysis, data curation, methodology.

Data availability The datasets generated during the current study are available from the corresponding author on reasonable request.

Declarations

Conflict of interest Authors declare no conflict of interest.

Ethical approval I'm the crossponding author and I declare that: *The manuscript should not be submitted to more than one journal for simultaneous consideration. * The authors agree to publish the manuscript in the journal of optical and quantum electronics.

References

Abouabassi, K., Atourki, L., Sala, A., Ouafi, M., Boulkaddat, L., Ait Hssi, A., Labchir, N., Bouabid, K., Almaggoussi, A., Gilioli, E.: Annealing effect on one step electrodeposited $CuSbSe_2$ thin films. Coatings **12**, 179–189 (2022)

Akcay, N., Gremenok, V., Ivanov, V.A., Zaretskaya, E., Ozcelik, S.: Characterization of Cu_2ZnSnS_4 thin films prepared with and without thin Al_2O_3 barrier layer. Sol. Energy **234**, 137–151 (2022)

Akl, A.A., Hassanien, A.S.: Microstructure characterization of Al–Mg alloys by X-ray diffraction line profile analysis. Int. J. Adv. Res. **2**, 1–9 (2014)

Akl, A.A., Hassanien, A.S.: Comparative microstructural studies using different methods: effect of Cd-addition on crystallography, microstructural properties, and crystal imperfections of annealed nano-structural thin $Cd_xZn_{1-x}Se$ films. Phys. B Condens. Matter. **620**, 413267 (2021)

Akl, A.A., El Radaf, I.M., Hassanien, A.S.: Intensive comparative study using X-ray diffraction for investigating microstructural parameters and crystal defects of the novel nanostructural $ZnGa_2S_4$ thin films. Superlattices Microstruct. **143**, 106544 (2020)

Akl, A.A., El Radaf, I.M., Hassanien, A.S.: An extensive comparative study for microstructural properties and crystal imperfections of novel sprayed Cu_3SbSe_3 nanoparticle-thin films of different thicknesses. Optik **227**, 165837 (2021)

Ali, H.A.M., El-Nahass, M.M., El-Zaidia, E.F.M.: Optical and dispersion properties of thermally deposited phenol red thin films. Opt. Laser Technol. **107**, 402–407 (2018). https://doi.org/10.1016/j.optlastec.2018.06.001

Aly, K.A.: Optical band gap and refractive index dispersion parameters of $As_xSe_{70}Te_{30-x}$($0 \le x \le 30$ at.%) amorphous films. Appl. Phys. A **99**, 913–919 (2010)

Alzaid, M., Qasem, A., Shaaban, E.R., Hadia, N.M.A.: Extraction of thickness, linear and nonlinear optical parameters of $Ge_{20+x}Se_{80-x}$ thin films at normal and slightly inclined light for optoelectronic devices. Opt. Mater.**110**, 110539 (2020)

Behera, M., Mishra, N.C., Naik, R.: Bismuth thickness-dependent structural and electronic properties of Bi/As_2Se_3 bilayer thin films. Indian J. Phys. **94**, 469–475 (2020)

Chalapathi, U., Bhaskar, P.U., Cheruku, R., Sambasivam, S., Park, S.-H.: Evolution of large-grained $CuSbS_2$ thin films by rapid sulfurization of evaporated Cu–Sb precursor stacks for photovoltaics application. Ceram. Int. (2022). https://doi.org/10.1016/j.ceramint.2022.09.365

Das, S., Mahanandia, P.: Improved PCE of solution processed kesterite Ag_2ZnSnS_4 quantum dot photovoltaic cell. Mater. Chem. Phys. **281**, 125878 (2022)

Das, S., Senapati, S., Alagarasan, D., Varadharajaperumal, S., Ganesan, R., Naik, R.: Enhancement of nonlinear optical parameters upon phase transition in new quaternary $Ge_{20}Ag_{10}Te_{10}Se_{60}$ films by annealing at various temperatures for optoelectronic applications. J. Alloys Compd. **927**, 167000 (2022)

Das, S., Senapati, S., Alagarasan, D., Ganesan, R., Varadharajaperumal, S., Naik, R.: Modifications in the structural, morphological, optical properties of $Ag_{45}Se_{40}Te_{15}$ thin films by proton ion irradiation for optoelectronics and nonlinear applications. Ceram. Int. **49**, 10319–10331 (2023)

Dughaish, Z.H., Mohamed, S.H.: Evaluation of optical constants of Tl_4PbTe_3 thin films with different thicknesses. Indian J. Phys. **87**, 741–746 (2013)

El Radaf, I.M.: Dispersion parameters, linear and nonlinear optical analysis of the $SnSb_2S_4$ thin films. Appl. Phys. A Mater. Sci. Process. **126**, 357 (2020a). https://doi.org/10.1007/s00339-020-03543-0

El Radaf, I.M.: Structural, optoelectrical, linear, and nonlinear optical characterizations of the $Cu_2ZnGeSe_4$ thin films. J. Mater. Sci. Mater. Electron. **31**, 3228–3237 (2020b). https://doi.org/10.1007/s10854-020-02871-4

El Radaf, I.M.: Synthesis and characterizations of p-type kesterite Ag_2ZnSnS_4 Thin Films Deposited by Spray Pyrolysis. J. Electron. Mater. (2020c). https://doi.org/10.1007/s11664-020-08063-4

El Radaf, I.M.: Facile synthesis, structural, optical and optoelectrical characterizations of promising novel $InSbS_3$ thin films for photovoltaic applications. Phys. B Condens. Matter. **650**, 414539 (2023)

El Radaf, I.M., Abdelhameed, R.M.: Surprising performance of graphene oxide/tin dioxide composite thin films. J. Alloys Compd. **765**, 1174–1183 (2018). https://doi.org/10.1016/j.jallcom.2018.06.277

El Radaf, I.M., Al-Zahrani, H.Y.S.: Facile Synthesis and Structural, Linear and Nonlinear Optical Investigation of p-type Cu2ZnGeS4 Thin Films as a Potential Absorber Layer for Solar Cells. J. Electron. Mater. **49**, 4843–4851 (2020). https://doi.org/10.1007/s11664-020-08204-9

El Radaf, I.M., Al-Zahrani, H.Y.S.: Structural, optical, and optoelectrical studies of spray pyrolyzed $CuGaSnS_4$ Thin Films. ECS J. Solid State Sci. Technol. **10**, 123012 (2021)

El Radaf, I.M., Al-Zahrani, H.Y.S.: Structural and optical studies of the novel $BiSbS_3$ thin films prepared by chemical bath deposition technique. Phys. B Condens. Matter. **631**, 413655 (2022)

El Radaf, I.M., Wassel, A.R.: Structural and optical characterizations of the thermally evaporated $Pb_xGa_{1-x}Se$ thin films. Optik **238**, 166610 (2021). https://doi.org/10.1016/j.ijleo.2021.166610

El Radaf, I.M., Fouad, S.S., Ismail, A.M., Sakr, G.B.: Influence of spray time on the optical and electrical properties of $CoNi_2S_4$ thin films. Mater. Res. Express. (2018). https://doi.org/10.1088/2053-1591/aaba0a

El Radaf, I.M., Hameed, T.A., El komy, G.M., Dahy, T.M.: Synthesis, structural, linear and nonlinear optical properties of chromium doped SnO_2 thin films. Ceram. Int. **45**, 3072–3080 (2019). https://doi.org/10.1016/j.ceramint.2018.10.189

El Radaf, I.M., Al-Zahrani, H.Y.S., Hassanien, A.S.: Novel synthesis, structural, linear and nonlinear optical properties of p-type kesterite nanosized Cu_2MnGeS_4 thin films. J. Mater. Sci. Mater. Electron. **31**, 8336–8348 (2020). https://doi.org/10.1007/s10854-020-03369-9

El-Bana, M.S., El Radaf, I.M.: Exploring the amorphous optical nature of $CuSbSe_2$ thin films, and investigating a promising photovoltaic ITO/CdS/CSS_2/Au heterojunction. Phys. B Condens. Matter. **632**, 413705 (2022)
El-Denglawey, A., Aly, K.A., Dahshan, A., Hassanien, A.S.: Optical characteristics of thermally evaporated thin a-$(Cu_2ZnGe)_{50-x}Se_{50+x}$ films. ECS J. Solid State Sci. Technol. **11**, 44006 (2022)
Fouad, S., El Radaf, I., Sharma, P., El-Bana, M.: Multifunctional CZTS thin films: structural, optoelectrical, electrical and photovoltaic properties. J. Alloys Compd. **757**, 124–133. (2018). https://doi.org/10.1016/j.jallcom.2018.05.033
Gao, Y., Zhao, L.: Review on recent advances in nanostructured transition-metal-sulfide-based electrode materials for cathode materials of asymmetric supercapacitors. Chem. Eng. J. **430**, 132745 (2022)
Ghosh, T., Kandpal, S., Rani, C., Bansal, L., Kumar, R.: Electrochromic strategies for modulation between primary colors: covering the visible spectrum. ACS Appl. Opt. Mater. **1**, 915–923 (2023). https://doi.org/10.1016/j.spmi.2020.106544
Göde, F.: Annealing temperature effect on the structural, optical and electrical properties of ZnS thin films. Phys. B Condens. Matter. **406**, 1653–1659 (2011)
Golan, G., Axelevitch, A., Gorenstein, B., Manevych, V.: Hot-probe method for evaluation of impurities concentration in semiconductors. Microelectronics J. **37**, 910–915 (2006)
Habiboglu, C., Erken, O., Gunes, M., Yilmaz, O., Cevlik, H.C., Ulutas, C., Gumus, C.: Effect of molar concentration on the structural, linear and nonlinear optical properties of CuS (covellite) thin films. Solid State Commun. **352**, 114823 (2022)
Hassanien, A.S.: Studies on dielectric properties, opto-electrical parameters and electronic polarizability of thermally evaporated amorphous $Cd_{50}S_{50-x}Se_x$ thin films. J. Alloys Compd. **671**, 566–578 (2016)
Hassanien, A.S.: Intensive linear and nonlinear optical studies of thermally evaporated amorphous thin Cu–Ge–Se–Te films. J. Non Cryst. Solids **586**, 121563 (2022)
Hassanien, A.S., El Radaf, I.M.: Optical characterizations of quaternary Cu_2MnSnS_4 thin films: novel synthesis process of film samples by spray pyrolysis technique. Phys. B Condens. Matter. **585**, 412110 (2020). https://doi.org/10.1016/j.physb.2020.412110
Hassanien, A.S., Sharma, I.: Dielectric properties, Optoelectrical parameters and electronic polarizability of thermally evaporated a-Pb–Se–Ge thin films. Phys. B Condens. Matter. **622**, 413330 (2021). https://doi.org/10.1016/j.physb.2021.413330
Hassanien, A.S., Aly, K.A., Akl, A.A.: Study of optical properties of thermally evaporated ZnSe thin films annealed at different pulsed laser powers. J. Alloys Compd. **685**, 733–742 (2016)
Hassanien, A.S., Alamri, H.R., El Radaf, I.M.: Impact of film thickness on optical properties and optoelectrical parameters of novel $CuGaGeSe_4$ thin films synthesized by electron beam deposition. Opt. Quantum Electron. **52**, 1–18 (2020a)
Hassanien, A.S., Neffati, R., Aly, K.A.: Impact of Cd-addition upon optical properties and dispersion parameters of thermally evaporated $Cd_xZn_{1-x}Se$ films: discussions on bandgap engineering, conduction and valence band positions. Optik **212**, 164681 (2020b). https://doi.org/10.1016/j.ijleo.2020.164681
Hassanien, A.S., Sharma, I., Aly, K.A.: Linear and nonlinear optical studies of thermally evaporated chalcogenide a–Pb–Se–Ge thin films. Phys. B Condens. Matter. **613**, 412985 (2021)
Hathot, S.F., Abbas, S.I., AlOgaili, H.A.T., Salim, A.A.: Influence of deposition time on absorption and electrical characteristics of ZnS thin films. Optik**260**, 169056 (2022)
Jrad, A., Naouai, M., Ammar, S., Turki-Kamoun, N.: Chemical composition, structural, morphological, optical and luminescence properties of chemical bath deposited Fe: ZnS thin films. Opt. Mater.**123**, 111851 (2022)
Kajana, T., Pirashanthan, A., Velauthapillai, D., Yuvapragasam, A., Yohi, S., Ravirajan, P., Senthilnanthanan, M.: Potential transition and post-transition metal sulfides as efficient electrodes for energy storage applications. RSC Adv. **12**, 18041–18062 (2022)
Karsandık, Ö., Özdal, T., Kavak, H.: Influence of thickness and annealing temperature on properties of solution processed bismuth sulfide thin films. J. Mater. Sci. Mater. Electron. **33**, 18014–18027 (2022)
Li, B., Wang, F., Wang, K., Qiao, J., Xu, D., Yang, Y., Zhang, X., Lyu, L., Liu, W., Liu, J.: Metal sulfides based composites as promising efficient microwave absorption materials: a review. J. Mater. Sci. Technol. **104**, 244–268 (2022)
Liu, Y., Geng, L., Xue, Z., Song, Z., Xuan, D., Song, S., Zhao, Z.: Syntheses, crystal structures, photocatalysis, and photoelectric responses of quaternary sulfides $ACuZnS_2$ (A= K, Rb, Cs). Inorg. Chem. Commun. **146**, 110108 (2022)
Mohamed, S.H., El-Hagary, M., Emam-Ismail, M.: Thickness and annealing effects on the optoelectronic properties of ZnS films. J. Phys. D Appl. Phys. **43**, 75401 (2010)

Mohamed, M., Shaaban, E.R., Abd-el Salam, M.N., Abdel-Latief, A.Y., Mahmoud, S.A., Abdel-Rahim, M.A.: Investigation of the optical and electrical parameters of $As_{47.5}Se_{47.5}Ag_5$ thin films with different thicknesses for optoelectronic applications. Optik**178**, 1302–1312 (2019a). https://doi.org/10.1016/j.ijleo.2018.10.103

Mohamed, S.H., Hadia, N.M.A., Awad, M.A., Shaaban, E.R.: Effects of thickness and Ag layer addition on the properties of ZnS thin films. Acta Phys. Pol. **135**, 420–425 (2019b)

Naik, R., Ganesan, R.: Thickness effect on the optical properties of Bi/As_2S_3 bilayer thin films. J. Non Cryst. Solids **385**, 142–147 (2014)

Naik, R., Ganesan, R., Adarsh, K.V., Sangunni, K.S., Takats, V., Kokenyesi, S.: Light and heat induced interdiffusion in Sb/As_2S_3 nano-multilayered film. J. Non Cryst. Solids **355**, 1939–1942 (2009)

Naik, R., Ganesan, R., Sangunni, K.S.: Optical properties change with the addition and diffusion of Bi to As_2S_3 in the Bi/As_2S_3 bilayer thin film. J. Alloys Compd. **554**, 293–298 (2013)

Naik, R., Aparimita, A., Alagarasan, D., Varadharajaperumal, S., Ganesan, R.: Linear and nonlinear optical properties change in Ag/GeS heterostructure thin films by thermal annealing and laser irradiation. Opt. Quantum Electron. **52**, 1–18 (2020)

Priyadarshini, P., Das, S., Alagarasan, D., Ganesan, R., Varadharajaperumal, S., Naik, R.: Observation of high nonlinearity in Bi doped $BixIn_{35-x}Se_{65}$ thin films with annealing. Sci. Rep. **11**, 21518 (2021)

Qasem, A., Hassaan, M.Y., Moustafa, M.G., Hammam, M.A.S., Zahran, H.Y., Yahia, I.S., Shaaban, E.R.: Optical and electronic properties for As-60 at.% S uniform thickness of thin films: influence of Se content. Opt. Mater. **109**, 110257 (2020)

Qasem, A., Mostafa, M.S., Yakout, H.A., Mahmoud, M., Shaaban, E.R.: Determination of optical bandgap energy and optical characteristics of $Cd_{30}Se_{50}S_{20}$ thin film at various thicknesses. Opt. Laser Technol. **148**, 107770 (2022)

Sahoo, D., Priyadarshini, P., Dandela, R., Alagarasan, D., Ganesan, R., Varadharajaperumal, S., Naik, R.: Optimization of linear and nonlinear optical parameters in $As_{40}Se_{60}$ film by annealing at different temperature. Optik**219**, 165286 (2020)

Sahoo, D., Priyadarshini, P., Dandela, R., Alagarasan, D., Ganesan, R., Varadharajaperumal, S., Naik, R.: Investigation of amorphous-crystalline transformation induced optical and electronic properties change in annealed $As_{50}Se_{50}$ thin films. Opt. Quantum Electron. **53**, 1–25 (2021a)

Sahoo, D., Priyadarshini, P., Dandela, R., Alagarasan, D., Ganesan, R., Varadharajaperumal, S., Naik, R.: In situ laser irradiation: the kinetics of the changes in the nonlinear/linear optical parameters of $As_{50}Se_{40}Sb_{10}$ thin films for photonic applications. RSC Adv. **11**, 16015–16025 (2021b)

Shaaban, E.R., Hassaan, M.Y., Moustafa, M.G., Qasem, A., Ali, G.A.M.: Optical constants, dispersion parameters and non-linearity of different thickness of $As_{40}S_{45}Se_{15}$ thin films for optoelectronic applications. Optik **186**, 275–287 (2019)

Sharma, I., Hassanien, A.S.: Effect of Ge-addition on physical and optical properties of chalcogenide $Pb_{10}Se_{90-x}Ge_x$ bulk glasses and thin films. J. Non Cryst. Solids **548**, 120326 (2020). https://doi.org/10.1016/j.jnoncrysol.2020.120326

Sharma, P., Katyal, S.C.: Effect of tin addition on the optical parameters of thermally evaporated As–Se–Ge thin films. Mater. Chem. Phys. **112**, 892–897 (2008)

Sharma, I., Sharma, P., Hassanien, A.S.: Optical properties and optoelectrical parameters of the quaternary chalcogenide amorphous $Ge_{15}Sn_xS_{35-x}Te_{50}$ films. J. Non Cryst. Solids **590**, 121673 (2022)

Surucu, O., Isik, M., Terlemezoglu, M., Bektas, T., Gasanly, N.M., Parlak, M.: Temperature effects on optical characteristics of thermally evaporated CuSbSe2 thin films for solar cell applications. Opt. Mater.**133**, 113047 (2022)

Tauc, J., Grigorovici, R., Vancu, A.: Optical properties and electronic structure of amorphous germanium. Phys. Status Solidi **15**, 627–637 (1966)

Tian, Q., Wang, G., Zhao, W., Chen, Y., Yang, Y., Huang, L., Pan, D.: Versatile and low-toxic solution approach to binary, ternary, and quaternary metal sulfide thin films and its application in $Cu_2ZnSn(S,Se)_4$ solar cells. Chem. Mater. **26**, 3098–3103 (2014)

Vakalopoulou, E., Rath, T., Kräuter, M., Torvisco, A., Fischer, R.C., Kunert, B., Resel, R., Schröttner, H., Coclite, A.M., Amenitsch, H.: Metal sulfide thin films with tunable nanoporosity for photocatalytic applications. ACS Appl. Nano Mater. **5**, 1508–1520 (2022a)

Vakalopoulou, E., Rath, T., Warchomicka, F.G., Carraro, F., Falcaro, P., Amenitsch, H., Trimmel, G.: Honeycomb-structured copper indium sulfide thin films obtained via a nanosphere colloidal lithography method. Mater. Adv. **3**, 2884–2895 (2022b)

Vázquez-Barragán, N.E., Rodríguez-Rosales, K., Colunga-Saucedo, M., Pérez-García, C.E., Santos-Cruz, J., Pérez-García, S.A., Contreras-Puente, G., de Moure-Flores, F.: Influence of the substrate temperature on the formation of $CuSbSe_2$ thin films grown by pulsed laser deposition. Ceram. Int. **48**, 35031–35038 (2022)

Verma, C.S., Shukla, N., Bose, P.: A review on chemical bath deposition mediated synthesis of binary/ternary photoconductive metal sulfide thin films. ECS Trans. **107**, 19647 (2022)
Vinotha, K., Jayasutha, B., Abel, M.J., Vinoth, K.: In^{3+}-doped CuS thin films: physicochemical characteristics and photocatalytic property. J. Mater. Sci. Mater. Electron. **33**, 22862–22882 (2022)
Wang, D., Yang, Y., Guo, T., Xiong, X., Xie, Y., Li, K., Li, B., Ghali, M.: Effect of pulse bias voltages on performance of CdTe thin film solar cells prepared by pulsed laser deposition. Sol. Energy **213**, 118–125 (2021)
Wang, Y., Lv, S., Li, Z.: Review on incorporation of alkali elements and their effects in Cu (In, Ga) Se_2 solar cells. J. Mater. Sci. Technol. **96**, 179–189 (2022)
Wassel, A.R., El Radaf, I.M.: Synthesis and characterization of the chemically deposited SnS_{1-x} Se_x thin films: structural, linear and nonlinear optical properties. Appl. Phys. A **126**, 1–10 (2020)
Wemple, S.H.: Refractive-index behavior of amorphous semiconductors and glasses. Phys. Rev. B **7**, 3767–3777 (1973). https://doi.org/10.1103/PhysRevB.7.3767
Wemple, S.H., DiDomenico, M.: Behavior of the electronic dielectric constant in covalent and ionic materials. Phys. Rev. B **3**, 1338–1351 (1971). https://doi.org/10.1103/PhysRevB.3.1338
Yan, C., Huang, J., Sun, K., Johnston, S., Zhang, Y., Sun, H., Pu, A., He, M., Liu, F., Eder, K.: Cu_2ZnSnS_4 solar cells with over 10% power conversion efficiency enabled by heterojunction heat treatment. Nat. Energy **3**, 764–772 (2018)
Yin, K., Xu, X., Wang, M., Zhou, J., Duan, B., Shi, J., Li, D., Wu, H., Luo, Y., Meng, Q.: A high-efficiency (12.5%) kesterite solar cell realized by crystallization growth kinetics control over aqueous solution based Cu_2ZnSn (S, Se) 4. J. Mater. Chem. a. **10**, 779–788 (2022)